Thermal noise as a window into the quantum vacuum: Spatial patterns revealed by simple experiments

Sun-Hyun Youn *

Department of Physics, Chonnam National University, Gwangju, South Korea

(Received 2 May 2025; accepted 3 June 2025; published 20 June 2025)

We show that the spatial structure of electromagnetic vacuum fluctuations, predicted by quantum electrodynamics, can be indirectly observed using thermal noise at radio frequencies. Using simple laboratory equipment like coaxial cables and radio frequency splitters, we detect a clear suppression of thermal noise near conducting boundaries, mirroring the expected modulation of vacuum modes. This provides accessible, experimental evidence for quantum vacuum behavior without requiring advanced optics or cryogenics.

DOI: 10.1103/fyk5-nbwd

I. INTRODUCTION

The behavior of electromagnetic fields near a mirror surface is fundamentally altered by boundary conditions, leading to the formation of standing waves [1,2]. This, in turn, modifies the vacuum fluctuations, impacting phenomena like spontaneous emission [3–7]. While theoretical predictions suggest a reduction in vacuum fluctuations near a mirror, direct experimental verification in the optical regime has been challenging due to limitations in spatial resolution. Here, we propose and demonstrate an approach using radio frequency (RF) measurements of thermal noise to indirectly probe the spatial distribution of vacuum fluctuations near a mirror. We leverage the fact that thermal noise, dominant in the RF domain, populates the same electromagnetic modes dictated by the boundary conditions as vacuum fluctuations. By characterizing the spatial distribution of thermal noise, we infer the corresponding modification of vacuum modes and, consequently, the vacuum fluctuations.

When light, an electromagnetic wave, is incident upon a mirror, the electric field must vanish at the mirror surface (assuming a perfect conductor). For a plane wave propagating in the z-direction and a mirror in the xy-plane, this boundary condition results in a standing wave pattern. The electric field intensity is zero at integer multiples of half the wavelength from the mirror and reaches a maximum at odd integer multiples of a quarter wavelength. This principle forms the basis of optical resonators (cavities), where only specific wavelengths (resonant modes) satisfying the boundary conditions imposed by two mirrors can exist.

It is well-established that this modification of the electromagnetic field also affects the vacuum fluctuations, the zero-point energy of the electromagnetic field [1]. These vacuum fluctuations are linked to shot noise in optical measurements, and it has been demonstrated that they can be reduced below the standard quantum limit through nonlinear optical interactions [7]. In 1993, one of us theoretically predicted that the magnitude of vacuum fluctuations could be reduced near a mirror surface, simply due to the boundary conditions, without requiring nonlinear media [8]. While indirect evidence supporting this prediction was obtained [9], direct experimental verification in the optical domain has remained elusive due to the difficulty of achieving subwavelength spatial resolution in the direction of light propagation.

The fundamental properties of electromagnetic waves, including the modification of modes near a boundary, are not limited to the optical regime. We therefore propose an experimental approach in a different frequency domain, specifically the RF range, to overcome the limitations of optical measurements.

The vacuum fluctuations of a specific electromagnetic mode correspond to the lowest possible energy state of that mode, as defined by its frequency. To isolate and measure these vacuum fluctuations, one must eliminate all contributions from thermal noise and other external signals at the corresponding frequency. This condition can only be approached by cooling the system to absolute zero (0 K) and shielding it from any extrinsic electromagnetic interference.

A compelling question then arises: once a state composed solely of vacuum fluctuations has been established, how does the subsequent introduction of thermal noise manifest spatially in terms of energy distribution? At a given frequency, the thermal energy added to the system acts to further excite the electromagnetic mode that initially harbored only the vacuum fluctuation energy. This added excitation effectively modifies the population of the mode, leading to a new energy distribution shaped by both vacuum and thermal contributions.

Now, consider a resonator formed by two mirrors in thermal equilibrium with a reservoir. The electromagnetic field inside the resonator will also reach thermal equilibrium, with energy distributed according to Planck's law. However, crucially, the frequencies are no longer continuous but are

*Contact author: sunyoun@jnu.ac.kr

discrete, corresponding to the resonant modes of the cavity. The energy introduced by thermal noise will populate these discrete modes, adjusting the photon number in each mode to reach thermal equilibrium. In other words, photon creation or annihilation is always defined *with respect to a chosen set of spatial modes*, determined by boundary conditions or, experimentally, by cavities, waveguides, or well-collimated free-space beams [10]. Injecting monochromatic radiation of frequency ω_k therefore does not create a new field configuration *ab initio*; rather, it increases the excitation level of an already defined mode from $|n_k>$ to $|n_{k+1}>$, exactly as adding energy to a mechanical oscillator drives it to a higher eigenstate [11]. Coherent, thermal, or squeezed superpositions of such Fock states constitute the operational toolbox of modern quantum optics [12,13].

Our main idea is to investigate how thermal noise is distributed under specific boundary conditions, and, by characterizing the electromagnetic field modes that arise in such conditions, infer the properties of vacuum fluctuations. This inference is justified by the fact that, in quantum electrodynamics, the ground state of quantized electromagnetic field modes, defined by the given boundary conditions, exhibits vacuum fluctuations that share the same spatial characteristics as the modes themselves [11,12,14].

Therefore, by measuring the spatial distribution of RF thermal noise near a mirror, we can infer the spatial distribution of the vacuum modes near the mirror and, consequently, how the vacuum fluctuations are modified.

While direct measurement of vacuum fluctuations in the RF domain is challenging due to the overwhelming thermal noise, measuring the spatial variation of the thermal noise allows us to deduce how the vacuum modes are shaped near the mirror, providing indirect access to the behavior of vacuum fluctuations. This approach opens a new avenue for experimentally investigating quantum electrodynamic effects near boundaries, circumventing the limitations of optical measurements.

Our experimental configuration utilizes BNC cables, with one end modified to achieve a zero impedance, effectively creating a mirrorlike boundary condition. In a simplified scenario, an amplifier with a 50-Ω input impedance connected to a 50-Ω BNC cable of length L, terminated with a load impedance Z_L, would primarily detect thermal noise originating from the amplifier's input stage. The input impedance in this setup is well-described by transmission line theory, being a function of cable length and load impedance.

However, we interpret the observed thermal noise signal not merely as a passive measurement, but as a consequence of energy from the amplifier's input stage thermal noise exciting vacuum modes within the cable, leading to the formation of electromagnetic waves. Therefore, measuring the spatial characteristics of this thermally induced noise within the cable is equivalent to probing the spatial characteristics of the vacuum modes themselves, effectively providing a measurement of the vacuum noise's spatial properties within the cable environment.

In this work, we first characterized the frequency-dependent thermal noise by varying both the length of the BNC cable connected to the amplifier input and the termination impedance (0 and infinity). While varying cable length for a fixed frequency is possible, we chose to analyze thermal noise across a range of frequencies for a fixed cable length to determine the spatial distribution of electromagnetic waves within the cable. This provided a comprehensive characterization of the electromagnetic mode structure.

Furthermore, analogous to how a beam splitter (BS) combines and separates optical beams, RF splitters can also manipulate electromagnetic waves through reflection and transmission. We employed a 4 × 4 RF splitter, connecting BNC cables to two input ports to define specific electromagnetic modes. By characterizing the propagation of these modes through the splitter, we investigated the behavior of vacuum fluctuations in the presence of a mirrorlike boundary, analogous to studying vacuum fluctuations near a reflecting surface. This configuration allows us to probe how zero-point energy manifests in such a constrained RF environment.

II. SPATIAL MAPPING OF THERMAL NOISE IN COAXIALLY CONSTRAINED GEOMETRIES: PROBING VACUUM FLUCTUATION MODES

We consider a system comprising a voltage source (v_b) in series with an impedance (Z_b), connected to a transmission line of length L_A and characteristic impedance Z_0. The transmission line is terminated with a load impedance Z_l. While the voltage across the device can be determined using equivalent impedance methods, we present here an analysis based on the theory of propagating electromagnetic waves [15,16].

The voltage originating from v_b is initially divided at the input of the transmission line. Due to the series connection of Z_b and Z_0, the voltage appearing at the input of the transmission line (v_0) is given by [15,17]:

$$v_0 = v_b \frac{Z_0}{Z_b + Z_0}. \tag{1}$$

This voltage v_0 propagates along the transmission line of length L_A to the load impedance Z_l. At the load, a portion of the wave is reflected. The reflected wave travels back along the transmission line (length L_A) to the input of the device. The voltage of this first reflected wave arriving back at the input (v_{1m}) is:

$$v_{1m} = v_0 e^{-ikL_A} \Gamma_l e^{-ikL_A}, \tag{2}$$

where k is the wave number of the electromagnetic wave. The term Γ_l represents the reflection coefficient at the load ($\frac{Z_l - Z_0}{Z_l + Z_0}$). Upon reaching the input, this wave encounters the impedance Z_b, leading to a further reflection. The voltage of this reflected wave (v_{1p}) is:

$$v_{1p} = v_0 e^{-ikL_A} \Gamma_l e^{-ikL_A} \Gamma_b, \tag{3}$$

where The term Γ_b is the reflection coefficient at the source end ($\frac{Z_b - Z_0}{Z_b + Z_0}$).

At this stage, the total electromagnetic wave amplitude at the device input is the superposition of the initial wave and the first two reflected waves, $v_0 + v_{1m} + v_{1p}$.

However, v_{1p} subsequently propagates along the line, undergoes reflection at Z_l, returns to the input, and is partially reflected again by Z_b. This process of repeated propagation and reflection continues indefinitely. The resulting superposition of all these waves at the device input leads to the total

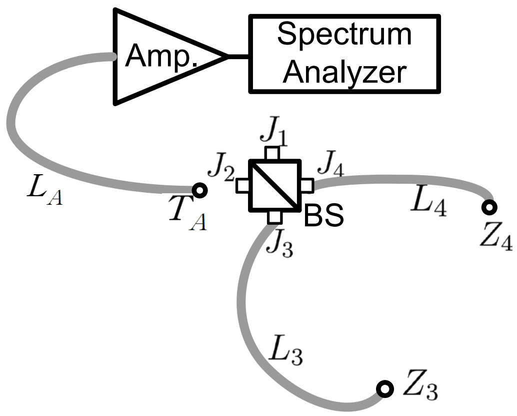

FIG. 1. Schematic of the noise measurement setup for a BNC cable. Noise amplified by a preamplifier is measured using a spectrum analyzer. The preamplifier is connected to a BNC cable of length L_A with a terminal impedance T_A. The sum and difference of the electromagnetic waves entering through terminals J_3 and J_4 of the beam splitter are transmitted to terminals J_1 and J_2, respectively. J_3 and J_4 are connected to BNC cables with terminal impedances Z_3 and Z_4 and lengths L_3 and L_4, respectively.

voltage v_s becomes

$$\begin{aligned} v_s &= v_0 + v_{1m} + v_{1p} + v_{2m} + v_{2p} + \cdots \\ &= v_0 \frac{e^{2ikL_A} + \Gamma_l}{e^{2ikL_A} - \Gamma_l \Gamma_b}. \end{aligned} \tag{4}$$

In the specific case where the device impedance matches the characteristic impedance of the transmission line ($Z_b = Z_0$), the reflection coefficient at the source end becomes zero. This eliminates all subsequent reflections from the source end, significantly simplifying the expression for v_s.

The magnitude squared of this simplified voltage, representing the power delivered to the device, is then:

$$v_s^2 = v_b^2 \frac{Z_l^2 \cos^2(kL_A) + Z_0^2 \sin^2(kL_A)}{(Z_0 + Z_l)^2}. \tag{5}$$

This expression can be recast in terms of the microwave frequency (f). The wave number (k) is related to the frequency by $k = \frac{2\pi f n}{c}$, where c is the speed of light in vacuum and n is the refractive index of the transmission line material:

$$v_s^2(f) = v_b^2 \frac{Z_l^2 \cos^2(2\pi f n L_A/c) + Z_0^2 \sin^2(2\pi f n L_A/c)}{(Z_0 + Z_l)^2}. \tag{6}$$

Prior to incorporating the BS (see Fig. 1), we conducted experiments varying both the length and termination impedance of the BNC cable connected to the preamplifier. Measurements were performed using an E4443A spectrum analyzer and an SR445 preamplifier at room temperature. The measured electromagnetic signal originated from thermal noise generated by the 50-Ω input impedance of the preamplifier. Cable lengths of 4 m and 8 m were tested, with the cable terminated in either a short circuit (0 Ω) or an open circuit (infinite impedance).

Figure 2 presents the measured noise power as a function of frequency for a 4-m BNC cable, comparing the cases of short-circuit and open-circuit termination against a 50-Ω matched termination. Red circles represent the short-circuit

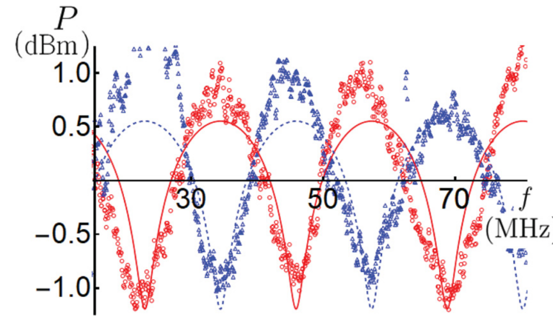

FIG. 2. Noise spectra measured using a spectrum analyzer, with the input BNC cable of the preamplifier set to a length of 4 m. Red circles and blue triangles indicate measurements taken with the cable end impedance set to 0 Ω and infinity, respectively. Values are normalized to the case where the cable end impedance is 50 Ω. Theoretical predictions (solid red and dashed blue lines) were calculated using a BNC cable with a length of 4.08 m and a refractive index of 1.60.

termination (0 Ω), while blue triangles represent the open-circuit termination (infinite impedance). The solid and dashed curves represent fits to the data, incorporating the preamplifier gain and system errors.

The quantity we aim to measure, $v_s^2(f)$, originates from the thermal noise generated at the input impedance of the preamplifier [18–20]. Within a given boundary condition, this thermal noise exhibits a frequency-dependent spatial distribution. However, the signal measured by the spectrum analyzer includes not only $v_s^2(f)$ but also various forms of environmental and instrumental noise.

Indeed, if there are additional losses in the BNC cable, thermal noise can be further introduced according to the fluctuation-dissipation theorem [21,22]. However, the resistive losses in the cable are much smaller than 50 Ω and are uniformly distributed along its length. As a result, the associated thermal noise contributes as a uniform background noise that does not significantly affect the frequency-dependent mode structure.

It is important to note that such additive background noise does not contribute to the reduction of thermal noise; rather, it increases the overall noise floor of the measured signal. Therefore, we performed a fitting of $v_s^2(f)$ in the low-noise region, where the noise power is minimal, and extended the fitting across the entire frequency range by introducing two fitting parameters: a system noise component (sn) and a relative gain factor of the measurement system (a).

The total measured signal, as recorded by the spectrum analyzer, is expressed as $(v_s^2 + sn) \cdot a$. Since the spectrum analyzer provides measurements in dBm, we converted the expression to a logarithmic scale. The final theoretical fitting function is given by:

$$f = 10 \log_{10} \left(a \left(v_s^2 + sn \right) \right). \tag{7}$$

Since multiple cables were connected in series to extend the total length, resulting in a cable length of several meters, a few centimeters of uncertainty in the total length were treated as a fitting parameter in the calculation of v_s^2. Optimization yielded $a = -1.754$, $sn = 1.91$, a cable length of 4.08 m,

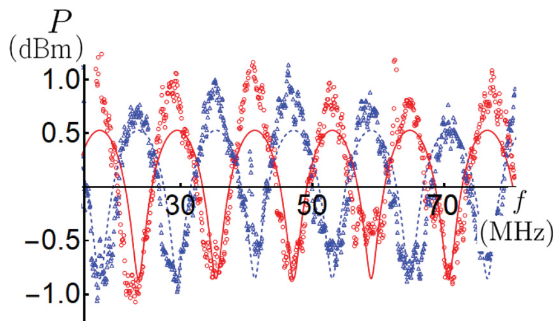

FIG. 3. Noise spectra measured using a spectrum analyzer, with the input BNC cable of the preamplifier set to a length of 8 m. Red circles and blue triangles indicate measurements taken with the cable end impedance set to 0 Ω and infinity, respectively. Values are normalized to the case where the cable end impedance is 50 Ω. Theoretical predictions (solid red and dashed blue lines) were calculated using a BNC cable with a length of 7.93 m and a refractive index of 1.60.

and a refractive index of $n = 1.60$. As evident in Fig. 2, the measured noise power exceeds the fitted values in regions of high noise. Conversely, in low-noise regions, the measured data aligns well with the theoretical predictions.

Figure 3 displays analogous results for an 8-m BNC cable, again comparing short-circuit (red circles) and open-circuit (blue triangles) terminations with a 50-Ω matched load. The solid and dashed curves represent fits using the same values for a, sn, and n as in Fig. 2, with only the cable length adjusted to 7.93 m for optimal fitting.

In this section, we experimentally investigate the spatial distribution of electromagnetic waves associated with thermal noise by directly connecting a BNC cable to the preamplifier and adjusting the impedance at the cable end to induce reflections of the propagating waves. The measured spatial profiles of the thermal noise show good agreement with theoretical predictions for cable lengths of 4 m and 8 m. Considering that thermal noise does not generate new spatial modes but rather excites existing electromagnetic modes, the spatial structure of thermal noise reflects the spatial characteristics of these modes, which, in turn, correspond to the spatial distribution of vacuum fluctuations. Therefore, our findings provide experimental insight into the spatial profile of vacuum fluctuations.

III. THERMAL NOISE DISTRIBUTION IN BS CONFIGURATIONS: INFERRING VACUUM FLUCTUATION SUPPRESSION

We analyze the propagation of electromagnetic waves and the contribution of thermal noise within a system incorporating a H2979 BS. The BS in Fig. 1 combines electromagnetic waves input at ports J_3 and J_4 to produce a sum signal output at port J_1 and a difference signal output at port J_2. A BNC cable of length L_A is connected directly to port J_2 for connection to the preamplifier. Port J_1 is terminated with a 50-Ω impedance to prevent reflections. BNC cables of lengths L_3 and L_4 are connected to ports J_3 and J_4, respectively, with characteristic impedances Z_3 and Z_4.

An initial voltage, v_{20}, applied to the input of a preamplifier, propagates along a cable of length L_A to port J_2 of the BS. The wave is then split and directed toward ports J_3 and J_4. The portion of the wave exiting J_4 travels along a cable, is reflected by an impedance Z_4, and subsequently splits again, propagating toward J_1 and J_2. A similar process occurs for the wave exiting J_3, reflecting from impedance Z_3 and splitting toward J_1 and J_2. Port J_1 is terminated with a 50-Ω impedance, matching that of the cable, preventing further reflections at this point. Therefore, the voltage at the preamplifier input resulting from the reflected waves via the BS can be expressed as:

$$v_{2a} = v_{20}[1 + e^{-ikL_A+i\omega\tau_{32}} s_{32}\Gamma_3 e^{-2ikL_3} e^{+i\omega\tau_{23}} s_{23} e^{-ikL_A} + e^{-ikL_A+i\omega\tau_{42}} s_{42}\Gamma_4 e^{-2ikL_4} e^{i\omega\tau_{24}} s_{24} e^{-ikL_A}], \tag{8}$$

where $\Gamma_i = (Z_i - Z_0)/(Z_i + Z_0)$ represents the reflection coefficient at impedance Z_i, Z_0 is the characteristic impedance of the cable, ω is the angular frequency, s_{ij} is the S-matrix of the BS, and τ_{ij} represents the propagation delay between ports i and j of the BS.

If the thermal noise generated by the resistor connected to the preamplifier is reflected back to the preamplifier through the region coupled via the BS and the associated cables, as described in Eq. (8), the thermal noise originating from the resistors located at the termination of the cables connected to the BS is transmitted to the preamplifier as given by Eq. (A4), which is derived in detail in the Appendix. This expression can be simplified by considering the limiting cases where Z_3 and Z_4 approach zero or infinity, yielding the following result:

$$v^2(m_3, m_4) = \frac{4k_bTZ_0}{8}\{4 - 2(-1)^{m_3}\cos(2(kL_A + kL_3 - \omega\tau_{23})) - 2(-1)^{m_4}\cos(2(kL_A + kL_4 - \omega\tau_{24})) - (-1)^{m_3+m_4}\cos(2kL_3 - 2kL_4 - \omega\tau_{13} + \omega\tau_{14} - \omega\tau_{23} + \omega\tau_{24}) + (-1)^{m_3+m_4}\cos(2(kL_3 - kL_4 - \omega\tau_{23} + \omega\tau_{24}))\}. \tag{9}$$

Here, m_i is an index representing the state of impedance Z_i, taking the value 0 when $Z_i = 0$ and 1 when $Z_i \to \infty$.

Figure 4 presents noise spectra measured at a spectrum analyzer connected to output port J_2 of a BS via a preamplifier, with specific cabling and termination conditions at the BS input and output ports. Input port J_3 is connected to a 2-m BNC cable terminated with a 0-Ω impedance, while input port J_4 is connected to a 1-m BNC cable terminated with an open circuit (infinite impedance). Output port J_1 is terminated with a 50-Ω impedance, matching the cable impedance. The green squares represent data acquired with a 2-m cable between J_1 and the preamplifier, and the blue triangles represent data with a 1-m cable in the same location. The data are presented as the noise power relative to that measured when the preamplifier input is terminated with a 50-Ω load. The solid green line is a fit to the data using Eq. (9) with the

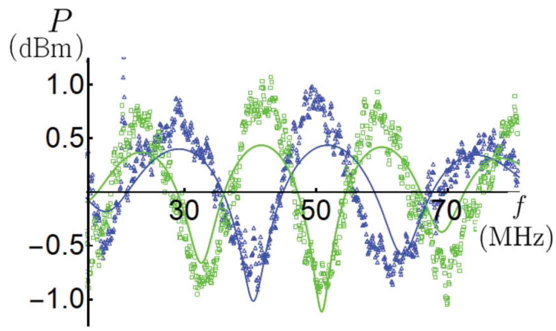

FIG. 4. Noise characteristics measured after the electromagnetic waves combined at the Beam Splitter (BS) were amplified by the preamplifier. A BNC cable with a length of 2 m and short-circuited impedance (0) was connected to terminal J_3 of the BS, while a BNC cable with a length of 1 m and an open-ended impedance (infinity) was connected to terminal J_4. The noise characteristics were measured for cases where the BNC cable length between the preamplifier and the BS was 2 m and 1 m, represented by green squares and blue triangles, respectively. Theoretical values calculated for cable lengths of 1.98 m and 0.98 m are shown as green and blue solid lines, respectively.

following parameters: $\tau_{41} = \tau_{31} = 5.31\,\text{ns}$, $\tau_{42} = \tau_{32} = 8.46\,\text{ns}$, $a = -1.27$, $s_n = 1.10$, and a distance of 0.98 m between the preamplifier and J_1. The solid blue line represents a fit with identical parameters, except for an increased preamplifier to J_1 distance of 1.98 m. The theoretical model shows good agreement in the low-noise regions, while discrepancies in high-noise regions are likely attributable to the intrusion of external noise sources.

To predict the characteristics of the thermal noise measured at the spectrum analyzer, as a function of BNC cable length at the BS input, theoretical calculations are presented in Fig. 5. The length of cable between J_2 and preamplifier is 2 m. The J_1 is terminated with 50 Ω. A 1-m BNC cable, terminated with an open circuit (infinite impedance), was connected to input port J_3. Another cable terminated to 0 Ω was connected to the other input port J_4. Calculations were performed for the noise

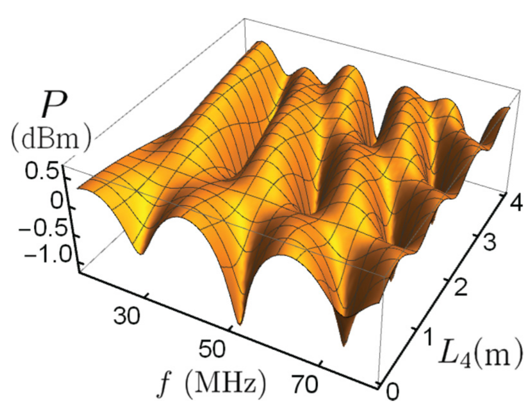

FIG. 5. Theoretical noise power as a function of frequency and BNC cable length at one input of a beam splitter (BS). The calculation assumes a 0-Ω impedance termination at input port J_4 (variable length cable). Input port J_3 has a fixed 1-m BNC cable terminated with infinite impedance (open circuit). The preamplifier is connected to the BS via a 2-m BNC cable.

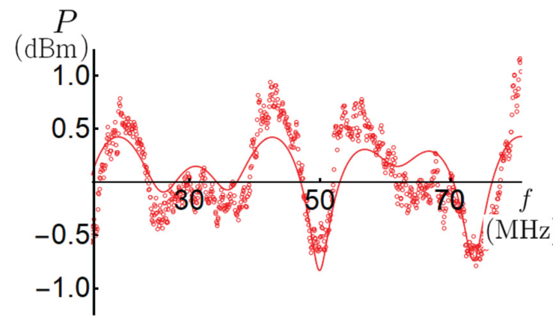

FIG. 6. Noise characteristics measured after the electromagnetic waves combined at the Beam Splitter (BS) were amplified by the preamplifier. A BNC cable with a length of 1 m and an open-ended impedance (infinity) was connected to terminal J_3 of the BS, while a BNC cable with a length of 4 m and a short-circuited impedance (0) was connected to terminal J_4. The BNC cable length between the preamplifier and the BS was 2 m. Theoretical values calculated for cable lengths of 1.98 m are shown as a red solid line.

power spectral density as a function of frequency, varying the length (L_4) of a BNC cable terminated in a short circuit (0 Ω) connected to input port J_4 from 0 to 4 meters. The calculations reveal complex interference patterns arising from reflections of electromagnetic waves within the cables connected to the BS input ports.

Figure 6 shows the calculated thermal noise power spectral density (red circles) for the case of $L_4 = 4\,\text{m}$ in Fig. 5. The red solid line is a fit to this calculated data, using the same parameters as in Fig. 4, but with a preamplifier to J_1 distance of 1.98 m and a cable length of 3.98 m connected to J_4. The data in the lower-noise regions are in strong agreement with the theoretical fit.

In this section, we experimentally investigate the spatial distribution of electromagnetic waves associated with thermal noise in several modes combined by the BS. The measured spatial profiles of the thermal noise show good agreement with theoretical predictions.

Thermal equilibrium of an object with its surroundings implies a balance between the object's internal thermal energy and the energy stored in the electromagnetic modes established by the environment. Consequently, the thermal noise originating from the object does not generate new electromagnetic modes within the environment; rather, it excites the pre-existing modes to maintain this equilibrium state.

Therefore, by examining the spatial distribution of electromagnetic waves originating from the resistor in the preamplifier within the BNC cable, one can infer the inherent electromagnetic mode structure of the BNC cable in the absence of these resistor-generated waves. This is because the electromagnetic waves due to thermal noise from the resistor do not alter the intrinsic modes of the BNC cable but merely excite them. As the temperature of the resistor decreases, the magnitude of the generated thermal noise diminishes. Extrapolating to 0 K, it is reasonable to surmise that the vacuum fluctuations, which would then be the dominant measurable quantity, would exhibit a similar spatial profile. For these reasons, measuring the thermal noise from the preamplifier resistor within the BNC cable setup incorporating the BS enables the prediction of vacuum fluctuations within a BNC cable terminated by a short circuit at one end. By extension, this approach suggests a method for inferring vacuum fluctuations in proximity to a mirror surface.

IV. DISCUSSION

In this work, we present an experiment that, while conceptually simple and implementable within a standard undergraduate physics laboratory, reveals striking insights into the spatial structure of quantum vacuum fluctuations. By measuring thermal noise propagating through BNC cables connected to a BS, we uncover the spatial distribution of electromagnetic modes shaped by the experimental boundary conditions. Although the data could be interpreted using conventional microwave impedance calculations at the preamplifier input, our approach instead emphasizes the coupling of thermal noise—originating from a 50-Ω resistor—into the spatially distributed electromagnetic modes supported by the surrounding environment.

Crucially, these measurements go beyond characterizing just thermal noise. The spatial pattern of the observed fluctuations mirrors the mode structure that would persist in the absence of thermal excitation—namely, the vacuum fluctuations dictated by quantum electrodynamics. In this sense, our simple setup offers a direct experimental window into the spatial distribution of quantum fluctuations, typically considered an abstract or inaccessible concept in undergraduate settings.

When the termination of the BNC cable is modified—for instance, by introducing a reflective short (0-Ω termination)—we observe changes in the standing wave patterns consistent with mirrorlike boundary conditions. This allows us to infer how vacuum fluctuations themselves are reshaped by spatial constraints. The experiment thus provides a rare opportunity to visualize how quantum noise is distributed in space, a phenomenon usually confined to high-precision quantum optics or condensed matter experiments.

That such a profound insight can arise from a thermal noise measurement using readily available laboratory equipment underscores the deep connection between classical noise and quantum fluctuations. While it might appear to be a reinterpretation of a textbook phenomenon, we argue that this perspective offers a more nuanced and spatially resolved understanding of vacuum fluctuations. This has significant implications for quantum-limited measurements—for example, in gravitational wave detection, where squeezed states are employed to suppress vacuum noise below the standard quantum limit.

The potential for practical applications is particularly compelling in the RF regime, where current technologies already allow precise control of boundary conditions. In intensity-stabilized light sources, for example, vacuum noise entering unused ports of BSs limits the achievable stability [23]. Our findings suggest that by incorporating reflective elements at these ports, specific components of quantum noise can be suppressed, enabling stabilization strategies that operate below the standard quantum limit—particularly in the RF domain, where subwavelength spatial resolution is readily accessible.

In summary, our experiment, though simple in execution, reveals the spatial distribution of quantum vacuum fluctuations shaped by boundary conditions, as inferred from thermal noise measurements. This unexpected depth of insight from an undergraduate-level setup highlights a broader principle: that quantum phenomena, far from being confined to exotic laboratories, can be probed and understood through careful reinterpretation of classical measurements. This approach opens new avenues for controlling and utilizing quantum noise across the electromagnetic spectrum.

ACKNOWLEDGMENTS

I would like to thank Heung-Ryul Noh for providing part of the equipment used in this study and the publication of this work was supported by Creation of the quantum information science R&D ecosystem (based on human resources, RS-2023-00256050) through the National Research Foundation of Korea (NRF) funded by the Korean government (Ministry of Science and ICT(MSIT)).

DATA AVAILABILITY

The data that support the findings of this article are not publicly available upon publication because it is not technically feasible, and/or the cost of preparing, depositing, and hosting the data would be prohibitive within the terms of this research project. The data are available from the author upon reasonable request.

APPENDIX: THERMAL NOISE CONTRIBUTIONS FROM PREAMPLIFIER INPUT RESISTANCE AND BEAM SPLITTER CABLE TERMINATIONS

To evaluate the propagation of thermal noise generated at the termination resistances of the cables connected to ports J_3, J_4, and J_1 of the BS to the input of the preamplifier, we begin by analyzing the contribution from the resistance Z_3 located at the end of the cable connected to port J_3. The resulting thermal noise contribution is given by:

$$v_{3a} = v_{30}e^{-ikL_3+i\omega\tau_{23}}s_{23}e^{-ikL_A}, \tag{A1}$$

where $v_{30} = \frac{Z_0}{Z_3+Z_0}\sqrt{4k_BTZ_3}$, representing the voltage noise spectral density at the source, with k_B being Boltzmann's constant and T the temperature.

Similarly, the thermal noise contribution from impedance Z_4 is:

$$v_{4a} = v_{40}e^{-ikL_4+i\omega\tau_{24}}s_{24}e^{-ikL_A}, \tag{A2}$$

where $v_{40} = \frac{Z_0}{Z_4+Z_0}\sqrt{4k_BTZ_4}$.

Finally, thermal noise originating from the termination impedance at J_1 propagates through the BS, with portions reaching the preamplifier input via J_2. This contribution is described by:

$$\begin{aligned} v_{1a} = v_{10}e^{-ikL_1}[&e^{+i\omega\tau_{31}}s_{31}\Gamma_3 s_{23}e^{-ikL_A+i\omega\tau_{23}} \\ &+ e^{i\omega\tau_{41}}s_{41}\Gamma_4 s_{24}e^{-ikL_A+i\omega\tau_{24}}], \end{aligned} \tag{A3}$$

where $v_{10} = \frac{Z_0}{Z_1+Z_0}\sqrt{4k_BTZ_1}$.

The S-matrix parameters characterizing the BS are: $s_{32} = s_{23} = -1/\sqrt{2}$ and $s_{24} = s_{42} = s_{31} = s_{13} = s_{14} = s_{41} = 1/\sqrt{2}$. The phase shift w_{ij} represents the propagation delay between ports i and j of the BS.

Considering the statistically independent nature of thermal noise sources, the total mean-squared voltage at the preamplifier input is:

$$
\begin{aligned}
v_{\text{sum}}^2 = {} & \frac{4k_bTZ_0}{8(Z_0+z_2)^2(Z_0+Z_3)^2(Z_0+Z_4)^2}(Z_0+z_2)^2\big\{Z_0^4+Z_3^2Z_4^2+4Z_0^3(Z_3+Z_4)+4Z_0Z_3Z_4(Z_3+Z_4)+Z_0^2\big(Z_3^2+12Z_3Z_4+Z_4^2\big) \\
& -\big(Z_0^2-Z_3^2\big)\big(Z_0^2-Z_4^2\big)\cos(2kL_3-2kL_4-\omega\tau_{13}+\omega\tau_{14}-\omega\tau_{23}+\omega\tau_{24})\big\} \\
& +4Z_0z_2\big\{3Z_0^4+4Z_0^3Z_3+3Z_0^2Z_3^2+4Z_0^3Z_4+4Z_0^2Z_3Z_4+4Z_0Z_3^2Z_4+3Z_0^2Z_4^2+4Z_0Z_3Z_4^2+3Z_3^2Z_4^2 \\
& -2\big(Z_0^2-Z_3^2\big)(Z_0+Z_4)^2\cos(2(kL_A+kL_3-\omega\tau_{23}))-2(Z_0+Z_3)^2\big(Z_0^2-Z_4^2\big)\cos(2(kL_A+kL_4-\omega\tau_{24})) \\
& +Z_0^4\cos(2(-kL_3+kL_4+\omega\tau_{23}-\omega\tau_{24}))-Z_0^2Z_3^2\cos(2(-kL_3+kL_4+\omega\tau_{23}-\omega\tau_{24})) \\
& -Z_0^2Z_4^2\cos(2(-kL_3+kL_4+\omega\tau_{23}-\omega\tau_{24}))+Z_3^2Z_4^2\cos(2(-kL_3+kL_4+\omega\tau_{23}-\omega\tau_{24}))\big\}. \qquad \text{(A4)}
\end{aligned}
$$

[1] H. B. G. Casimir, On the attraction between two perfectly conducting plates, Proc. Kon. Ned. Akad. Wetensch. **51**, 793 (1948).

[2] K. A. Milton, *The Casimir Effect: Physical Manifestations of Zero-Point Energy* (World Scientific, New Jersey, 2001).

[3] S. K. Lamoreaux, Demonstration of the Casimir force in the 0.6 to 6 μm range, Phys. Rev. Lett. **78**, 5 (1997).

[4] U. Mohideen and A. Roy, Precision measurement of the Casimir force from 0.1 to 0.9μm, Phys. Rev. Lett. **81**, 4549 (1998).

[5] S. Haroche and J.-M. Raimond, *Exploring the Quantum: Atoms, Cavities, and Photons* (Oxford University Press, 2006).

[6] C. I. Sukenik, M. G. Boshier, D. Cho, V. Sandoghdar, and E. A. Hinds, Measurement of the Casimir-Polder force, Phys. Rev. Lett. **70**, 560 (1993).

[7] W. Jhe, A. Anderson, E. A. Hinds, D. Meschede, L. Moi, and S. Haroche, Suppression of spontaneous decay at optical frequencies: Test of vacuum-field anisotropy in confined space, Phys. Rev. Lett. **58**, 666 (1987).

[8] S.-H. Youn, J.-H. Lee, and J.-S. Chang, Modulation of the vacuum field in the beam splitter and mirror system, Opt. Quant. Electron. **27**, 355 (1995).

[9] S. A. Wadood, J. T. Schultz, A. N. Vamivakas, and C. R. Stroud Jr., Do remote boundary conditions affect photodetection? J. Mod. Opt. **66**, 1116 (2019).

[10] C. Cohen-Tannoudji, J. Dupont-Roc, and G. Grynberg, *Photons and Atoms: Introduction to Quantum Electrodynamics* (Wiley, 1989).

[11] M. O. Scully and M. S. Zubairy, *Quantum Optics* (Cambridge University Press, 1997), Chap. 1.

[12] R. Loudon, *The Quantum Theory of Light*, 3rd ed. (Oxford University Press, 2000).

[13] C. W. Gardiner and P. Zoller, *Quantum Noise*, 3rd ed. (Springer, 2004).

[14] A. Yariv, *Quantum Electronics*, 3rd ed. (John Wiley & Sons, New York, 1997), Chap. 5.

[15] D. M. Pozar, *Microwave Engineering*, 4th ed. (John Wiley & Sons, Hoboken, 2011).

[16] E. Shahmoon, Casimir forces in transmission-line circuits: QED and fluctuation-dissipation formalisms, Phys. Rev. A **95**, 062504 (2017).

[17] M. Zahn, Electromagnetic Field Theory: A Problem Solving Approach, LibreTexts Engineering, Massachusetts Institute of Technology via MIT OpenCourseWare (2023), online available, https://eng.libretexts.org/.

[18] J. B. Johnson, Thermal agitation of electricity in conductors, Phys. Rev. **32**, 97 (1928).

[19] H. Nyquist, Thermal agitation of electric charge in conductors, Phys. Rev. **32**, 110 (1928).

[20] P. Horowitz and W. Hill, *The Art of Electronics*, 3rd ed. (Cambridge University Press, Cambridge, 2015).

[21] R. Kubo, The fluctuation-dissipation theorem, Rep. Prog. Phys. **29**, 255 (1966).

[22] H. B. Callen and T. A. Welton, Irreversibility and generalized noise, Phys. Rev. **83**, 34 (1951).

[23] S.-H. Youn, W. Jhe, J.-H. Lee, and J.-S. Chang, Effect of vacuum fluctuations on the quantum-mechanical amplitude noise of a laser diode in feedback systems, J. Opt. Soc. Am. B **11**, 102 (1994).